Are we overlooking lepton-flavor-universal new physics in $b \to s\ell\ell$?

Marcel Algueró,[1,2] Bernat Capdevila,[1,2] Sébastien Descotes-Genon,[3] Pere Masjuan,[1,2] and Joaquim Matias[1,2]

[1]*Grup de Física Teòrica (Departament de Física), Universitat Autònoma de Barcelona,*
E-08193 Bellaterra (Barcelona), Spain
[2]*Institut de Física d'Altes Energies (IFAE), The Barcelona Institute of Science and Technology,*
Campus UAB, E-08193 Bellaterra (Barcelona), Spain
[3]*Laboratoire de Physique Théorique, UMR 8627, CNRS, Univ. Paris-Sud, Université Paris-Saclay,*
91405 Orsay Cedex, France

The deviations with respect to the Standard Model that are currently observed in $b \to s\ell\ell$ transitions (the so-called flavor anomalies) can be interpreted in terms of different new physics (NP) scenarios within a model-independent effective approach. We reconsider the determination of NP in global fits from a different perspective by removing one implicit hypothesis of current analyses, namely, that NP is only lepton-flavor-universality violating (LFUV). We examine the roles played by LFUV NP and lepton-flavor-universal NP altogether, providing new directions to identify the possible theory beyond the SM responsible for the anomalies observed. New patterns of NP emerge due to the possibility of allowing at the same time large LFUV and lepton-flavor-universal NP contributions to $\mathcal{C}_{10\mu}$, which provides a different mechanism to obey the constraint from the $B_s \to \mu^+\mu^-$ branching ratio. In this landscape of NP, we discuss how to discriminate among these scenarios in the short term, thanks to current and forthcoming observables. While the update of R_K will be a major milestone to confirm the NP origin of the flavor anomalies, additional observables, in particular the LFUV angular observable Q_5, turn out to be central to assessing the precise NP scenario responsible for the observed anomalies.

I. INTRODUCTION

Besides the fundamental discovery of the Standard Model (SM) Higgs, the first run at the LHC had two clear outcomes. On one side, no signals of new physics (NP) have been found in direct searches. On the other side, indirect searches have led to a large set of deviations with respect to the SM (or anomalies) in both $b \to c\ell\nu$ and in $b \to s\ell\ell$ decays [1–3]. We can classify the latter (which we focus on) in two sets: $b \to s\mu\mu$ anomalies related to observables testing only muonic transitions, which we call lepton-flavor dependent (LFD), and lepton-flavor-universality violating (LFUV) anomalies that correspond to deviations in observables comparing muonic and electronic transitions.

The $b \to s\ell\ell$ anomalies have been analyzed in the effective Hamiltonian approach, which separate short- and long-distance contributions in a model-independent way (see, for instance, Ref. [4]). The analysis now combines the experimental data from LHC experiments (LHCb [5–9] but also ATLAS [10] and CMS [11]) as well as the data from B factories (in particular, Belle [12,13]) together with theoretical input concerning long-distance hadronic contributions [14–17]. They aim at extracting the value of the short-distance Wilson coefficients under given NP hypotheses and at comparing them with the SM expectations. Even though different global analyses in the literature use different approaches (statistical treatment, observables, hadronic inputs, etc.), they agree on the emerging global picture [18–24]. For instance, in Ref. [19], a global fit including both LFD and LFUV observables finds pulls (comparing the statistical significance of the SM against that of a NP hypothesis) between 5.0 and 5.8σ, depending on the particular NP hypothesis used. The LFUV NP hypotheses involving either $\mathcal{C}_{9\mu}^{\text{NP}}$ or $\mathcal{C}_{9\mu}^{\text{NP}} = -\mathcal{C}_{10\mu}^{\text{NP}}$ are among those with the highest significances.

In this paper, we consider the possibility that short-distance Wilson coefficients will receive contributions from NP that are not only LFUV but also lepton-flavor universal. Indeed, whereas LFUV NP contributions are mandatory to explain R_K and R_{K^*}, $b \to s\ell\ell$ processes are not restricted to such NP contributions alone. While several articles [19–24] allowed the presence of NP in electrons in

global fits to $b \to s\ell\ell$, in the present paper, we go one step beyond, and we impose different types of LFU structures between all leptons. We show that a universal LFU NP contribution, together with a LFUV NP contribution, gives rise to scenarios with a statistical significance at least as relevant as the ones identified in Ref. [19], against a common belief that the presence of such terms is not justified from the statistical point of view and should be dropped. This may help motivate the construction of new models including not only LFUV but also LFU NP contributions. Thus, we reconsider the results of the fit, allowing for the presence of two different types of NP that may lead to a new paradigm concerning the nature of the underlying theory beyond the SM. We then discuss the next steps, to identify the NP scenario that is realized in nature among the ones already favored, complementing Refs. [16,19]. Following our findings, the UV completion of the SM may require significant contributions from two different sectors (LFU and LFUV) instead of a single one, as often assumed.

II. TWO TYPES OF NP CONTRIBUTIONS

The $b \to s\ell\ell$ processes can be analyzed within the effective Hamiltonian framework [25,26]. The observables for exclusive decays can be written as interference terms between helicity amplitudes which are given as (short-distance) Wilson coefficients multiplying (long-distance) hadronic matrix elements [27–29], with a separation between short and long distances given by the factorization scale $\mu_b = O(m_b)$. One can use the fact that m_b is significantly larger than the typical QCD scale in order to isolate perturbatively computable contributions to the hadronic matrix elements (using effective approaches like QCD factorization). These perturbative contributions of hadronic origin can be lumped together with the purely short-distance contribution into effective Wilson coefficients (that will multiply nonperturbative hadronic form factors) with the structure in the case of $B \to K^{(*)}\ell\ell$ [30]

$$\mathcal{C}_{9\ell}(q^2) = \mathcal{C}_{9\,\text{pert}}^{\text{SM}}(q^2) + \mathcal{C}_9^{c\bar{c}}(q^2) + \mathcal{C}_{9\ell}^{\text{NP}}$$
$$\mathcal{C}_{10\ell} = \mathcal{C}_{10}^{\text{SM}} + \mathcal{C}_{10\ell}^{\text{NP}}, \tag{1}$$

where $\ell = e, \mu$. The short-distance SM values [31] at this scale $\mu_b = 4.8$ GeV are $\mathcal{C}_9^{\text{SM}} = 4.07$ and $\mathcal{C}_{10}^{\text{SM}} = -4.31$. We have $\mathcal{C}_{9\,\text{pert}}^{\text{SM}} = \mathcal{C}_9^{\text{SM}} + Y(q^2)$, where the function $Y(q^2)$ stems from one-loop matrix elements of four-quark operators $\mathcal{O}_{1-6}$, corresponding to the $c\bar{c}$ continuum. It can be evaluated within perturbation theory at leading order, and corrections at $\mathcal{O}(\alpha_s)$ to $\mathcal{C}_{9\ell}$ to this function are known [30,32,33]. In addition to this continuum, there is a long-distance contribution, which corresponds in particular to charmonium resonances $\mathcal{C}_9^{c\bar{c}}$ and depends on the external hadron state. Several approaches are available to estimate this contribution [17,22,34], all with similar outcomes [16,24]. Here, we follow Refs. [4,16], using the light-cone

sum rule computation with one soft-gluon exchange [14] to get an order of magnitude estimate of this contribution, without making any assumption about its sign and thus allowing for constructive or destructive interference with the other contributions to $\mathcal{C}_{9\mu}$.

This effective approach is the basis for global fits to the data in order to constrain the NP contributions $\mathcal{C}_{i\ell}^{\text{NP}}$ under various NP assumptions [19–22,24]. It turns out that the combination of anomalies in some LFD ($b \to s\mu\mu$) angular observables and in LFUV ratios R_K and R_{K^*} selects hypotheses with a large NP contribution to the Wilson coefficient $\mathcal{C}_{9\mu}$ (of order 25% of the SM) or NP contributions to both $\mathcal{C}_{9\mu}$ and $\mathcal{C}_{10\mu}$.

Following this perspective, we ought to be more precise on what goes under the "new physics" landscape. In this paper, we consider that the short-distance Wilson coefficients $\mathcal{C}_{i\mu}$ can contain two types of NP contribution,

$$\mathcal{C}_{i\ell}^{\text{NP}} = \mathcal{C}_{i\ell}^{\text{V}} + \mathcal{C}_i^{\text{U}}, \tag{2}$$

with $\ell = e, \mu$ (the extension to τ is trivial, assuming true universality among e, μ, and τ), where $\mathcal{C}_{i\ell}^{\text{V}}$ stands for lepton-flavor-universality violating NP and $\mathcal{C}_i^{\text{U}}$ stands for lepton-flavor-universal NP contributions. These short-distance contributions are all independent of the external hadronic states and their kinematics; they differ therefore from long-distance hadronic contributions, which are LFU but dependent on the nature and kinematics of the hadronic states. We will define the separation between the two types of contributions by imposing that LFUV contributions affect only muons

$$\mathcal{C}_{ie}^{\text{V}} = 0. \tag{3}$$

There is no loss of generality here, since this term can always be absorbed in such a way that $\mathcal{C}_{i\mu}^{\text{V}}$ can be interpreted as the difference of NP contributions to muons and electrons.

III. GLOBAL FITS IN THE PRESENCE OF LFU NP

LFUV NP contributions are mandatory to explain LFUV anomalies. The $b \to see$ measurements (in limited number, without significant deviations [13,35]) are compatible to no LFU-NP contributions (as often assumed), but they do not prevent these contributions from occurring. Assuming hadronic contributions properly assessed [16,24], we consider for the first time that LFU NP contributions can exist for both $\mathcal{C}_9$ and $\mathcal{C}_{10}$, together with LFUV NP contributions. It is important to remark that this is not the same as simply allowing for NP in electrons; we impose as a constraint in the fit that this contribution is the same for all leptons and work out the consequences of this identity. The key point to lift the degeneracy between the various contributions through the fit consists in considering together LFUV and LFD observables. The LFUV observables will

TABLE I. Scenario 3: 4D hypothesis with $\mathcal{C}_{9\mu}^{V}$ and $\mathcal{C}_{10\mu}^{V}$ and with $\mathcal{C}_{9}^{U}$ and $\mathcal{C}_{10}^{U}$.

	Best-fit point	1σ CI	2σ CI
$\mathcal{C}_{9\mu}^{V}$	0.08	$[-0.72, 0.80]$	$[-1.69, 1.49]$
$\mathcal{C}_{10\mu}^{V}$	1.14	$[0.66, 1.59]$	$[0.12, 2.03]$
$\mathcal{C}_{9}^{U}$	-1.26	$[-1.92, -0.25]$	$[-2.43, 1.62]$
$\mathcal{C}_{10}^{U}$	-0.91	$[-1.40, -0.40]$	$[-1.89, 0.16]$

TABLE II. Scenario 4: 3D hypothesis with $\mathcal{C}_{9\mu}^{V} = -\mathcal{C}_{10\mu}^{V}$ and with $\mathcal{C}_{9}^{U}$ and $\mathcal{C}_{10}^{U}$.

	Best-fit point	1σ CI	2σ CI
$\mathcal{C}_{9\mu}^{V} = -\mathcal{C}_{10\mu}^{V}$	-0.68	$[-0.96, -0.45]$	$[-1.28, -0.26]$
$\mathcal{C}_{9}^{U}$	-0.37	$[-0.68, -0.03]$	$[-0.95, 0.35]$
$\mathcal{C}_{10}^{U}$	-0.51	$[-0.86, -0.18]$	$[-1.24, 0.13]$

constrain LFUV NP contributions ($\mathcal{C}_{i\ell}^{V}$), whereas LFD observables will be sensitive to the sum of LFUV NP and LFU NP contributions ($\mathcal{C}_{i}^{U} + \mathcal{C}_{i\ell}^{V}$). As we increase the number of parameters, we have more flexibility to describe the data, which could lead to an improvement compared to our earlier fits restricted to LFUV NP contributions only and opens the possibility of new NP models.

We start from the results presented in the Table II of Ref. [19], for the global fits under (favored) one-dimensional (1D) hypotheses of NP in $b \to s\mu\mu$. The 1D hypothesis with $\mathcal{C}_{9\mu}^{NP}$ (scenario 1) led to a 68% confidence interval of $[-1.28, -0.94]$ with a pull with respect to the SM of 5.8σ, whereas the hypothesis $\mathcal{C}_{9\mu}^{NP} = -\mathcal{C}_{10\mu}^{NP}$ (scenario 2) had a 68% confidence interval of $[-0.75, -0.49]$ with a pull of 5.3σ. We consider now a set of nested fits named scenarios 3 to 8 and presented in Tables I–V in decreasing order of complexity to better understand the interplay between LFUV and LFU NP (more information and results, including the correlations among the parameters, are given in the Appendix A and B):

(i) The general hypothesis $\{\mathcal{C}_{9\mu}^{V}, \mathcal{C}_{10\mu}^{V}, \mathcal{C}_{9}^{U}, \mathcal{C}_{10}^{U}\}$ (Table I) has a pull of 5.6σ with respect to the SM. The result is remarkable: considering the best-fit point (b.f.p.), $\mathcal{C}_{9\mu}^{V}$ almost vanishes, $\mathcal{C}_{9,10}^{U}$ are far away from zero, and $\mathcal{C}_{10\mu}^{V}$ is larger than 1. At first glance, this result seems to contradict the previous global analyses

TABLE III. Scenario 5: 3D hypothesis with $\mathcal{C}_{9\mu}^{V}$ and $\mathcal{C}_{10\mu}^{V}$ and with $\mathcal{C}_{9}^{U} = \mathcal{C}_{10}^{U}$. Confidence Intervals (CI) are also provided.

	Best-fit point	1σ CI	2σ CI
$\mathcal{C}_{9\mu}^{V}$	-0.16	$[-0.94, 0.46]$	$[-2.05, 0.98]$
$\mathcal{C}_{10\mu}^{V}$	1.00	$[0.18, 1.59]$	$[-1.35, 2.06]$
$\mathcal{C}_{9}^{U} = \mathcal{C}_{10}^{U}$	-0.87	$[-1.43, -0.14]$	$[-1.91, 0.98]$

TABLE IV. Scenario 6: 2D hypothesis with $\mathcal{C}_{9\mu}^{V} = -\mathcal{C}_{10\mu}^{V}$ and $\mathcal{C}_{9}^{U} = \mathcal{C}_{10}^{U}$.

	Best-fit point	1σ CI	2σ CI
$\mathcal{C}_{9\mu}^{V} = -\mathcal{C}_{10\mu}^{V}$	-0.64	$[-0.77, -0.51]$	$[-0.90, -0.39]$
$\mathcal{C}_{9}^{U} = \mathcal{C}_{10}^{U}$	-0.44	$[-0.58, -0.29]$	$[-0.71, -0.14]$

(including Ref. [19]) and should be explained in more detail. The key observation is that $R_{K^{(*)}}$-like observables may be also accommodated by $\mathcal{C}_{10\mu}^{V}$ alone with a negligible $\mathcal{C}_{9\mu}^{V}$, cf. the Appendix A. This result was not obtained in the two-dimensional (2D) fits with only LFUV NP contributions (setting $\mathcal{C}_{i}^{U} = 0$), since LFD observables led then to the favored scenarios with b.f.p. $\mathcal{C}_{9\mu}^{V} \simeq -1$ and $\mathcal{C}_{9\mu}^{V} = -\mathcal{C}_{10\mu}^{V} \simeq -0.7$. Adding LFU contributions provides complementary mechanisms to explain LFUV and LFD anomalies. On one side, the LFD anomalies are accommodated by $\mathcal{C}_{9\mu}^{V} + \mathcal{C}_{9}^{U} \simeq -1.18$ and $\mathcal{C}_{10\mu}^{V} + \mathcal{C}_{10}^{U} \simeq +0.23$. On the other side, the LFUV observables are accommodated by $\mathcal{C}_{10\mu}^{V} \simeq 1.14$. It is thus not a surprise that the summed LFU and LFUV contributions for both $\mathcal{C}_{9,10}$ yield a result close to the fit to all observables under the NP hypothesis ($\mathcal{C}_{9\mu}^{NP}, \mathcal{C}_{10\mu}^{NP}$) shown in Table III of Ref. [19]. Under this hypothesis, $\mathcal{C}_{9\mu}^{V}$ changes sign with respect to fits without LFU in order to resolve the inner tensions between LFUV and LFD observables. Moreover, the constraint from $\mathcal{B}(B_s \to \mu^+\mu^-)$ is obeyed by the sum $\mathcal{C}_{10\mu}^{V} + \mathcal{C}_{10}^{U}$ with opposite signs, thus allowing a large $\mathcal{C}_{10\mu}^{V}$. This important feature is observed for the first time here and opens new possibilities for models beyond the SM.

(ii) The hypothesis $\{\mathcal{C}_{9\mu}^{V} = -\mathcal{C}_{10\mu}^{V}, \mathcal{C}_{9}^{U}, \mathcal{C}_{10}^{U}\}$ (Table II) is model-building motivated for theories with a significant scale gap between SM and NP [36–40], as the additional NP contributions should be invariant under $SU(2)_L$. Remarkably, this three-dimensional (3D) fit has a pull of 5.7σ to SM. The b.f.p. is in good agreement with the result found in Table II of Ref. [19] but with LFU contributions differing from zero at the 1σ level. The increase in the SM pull with respect to the case without LFU (5.7σ vs 5.3σ [19], with two more parameters) hints at a slight preference for LFU NP in both $\mathcal{C}_{9,10}$.

(iii) The hypothesis $\{\mathcal{C}_{9\mu}^{V}, \mathcal{C}_{10\mu}^{V}, \mathcal{C}_{9}^{U} = \mathcal{C}_{10}^{U}\}$ (Table III) is inspired by the fit in Table I, which suggests $\mathcal{C}_{9}^{U} \simeq \mathcal{C}_{10}^{U}$. We find Table III with a pull of 5.8σ with respect to the SM, slightly larger than the four-dimensional (4D) hypothesis.

(iv) The hypothesis $\{\mathcal{C}_{9\mu}^{V} = -\mathcal{C}_{10\mu}^{V}, \mathcal{C}_{9}^{U} = \mathcal{C}_{10}^{U}\}$ (Table IV) combines the suggestive results from both Tables I

TABLE V.　2D hypotheses. Top: Scenario 7: LFUV and LFU NP in $\mathcal{C}^{\mathrm{NP}}_{9\ell}$ only. Bottom: Scenario 8: $\mathcal{C}^{\mathrm{V}}_{9\mu} = -\mathcal{C}^{\mathrm{V}}_{10\mu}$ and $\mathcal{C}^{\mathrm{U}}_9$ only.

	Best-fit point	1σ CI	2σ CI
$\mathcal{C}^{\mathrm{V}}_{9\mu}$	-1.57	$[-2.14, -1.06]$	$[-2.75, -0.58]$
$\mathcal{C}^{\mathrm{U}}_9$	0.56	$[0.01, 1.15]$	$[-0.51, 1.78]$
$\mathcal{C}^{\mathrm{V}}_{9\mu} = -\mathcal{C}^{\mathrm{V}}_{10\mu}$	-0.42	$[-0.57, -0.27]$	$[-0.72, -0.15]$
$\mathcal{C}^{\mathrm{U}}_9$	-0.67	$[-0.90, -0.42]$	$[-1.11, -0.16]$

and III and yields a fit with a pull of 6.0σ with respect to the SM. The b.f.p. $\mathcal{C}^{\mathrm{V}}_{9\mu} = -\mathcal{C}^{\mathrm{V}}_{10\mu} = -0.64$ obtained now is very similar to the one from Table II, and $\mathcal{C}^{\mathrm{U}}_9 = \mathcal{C}^{\mathrm{U}}_{10} = -0.44$ is exactly the average of LFU contributions found in Table II. This particular 2D correlation is shown in Fig. 1 (see the Appendix B for correlations under the other hypotheses). It is interesting that a $\mathcal{C}_{10}$ contribution gives rise to a rather tight 1σ confidence interval, mainly due to $\mathcal{B}(B_s \to \mu^+\mu^-)$. Let us add that the hypothesis $\{\mathcal{C}^{\mathrm{V}}_{9\mu} = -\mathcal{C}^{\mathrm{V}}_{10\mu}, \mathcal{C}^{\mathrm{U}}_9 = -\mathcal{C}^{\mathrm{U}}_{10}\}$ [once again of interest for models based on $SU(2)_L$ invariance] has a pull with respect to the SM lower by almost 1σ and is not favored by the data, as can already be seen in Table I.

Two additional 2D hypotheses provide a bridge between the above hypotheses with LFU NP in both $\mathcal{C}_{9,10}$ and
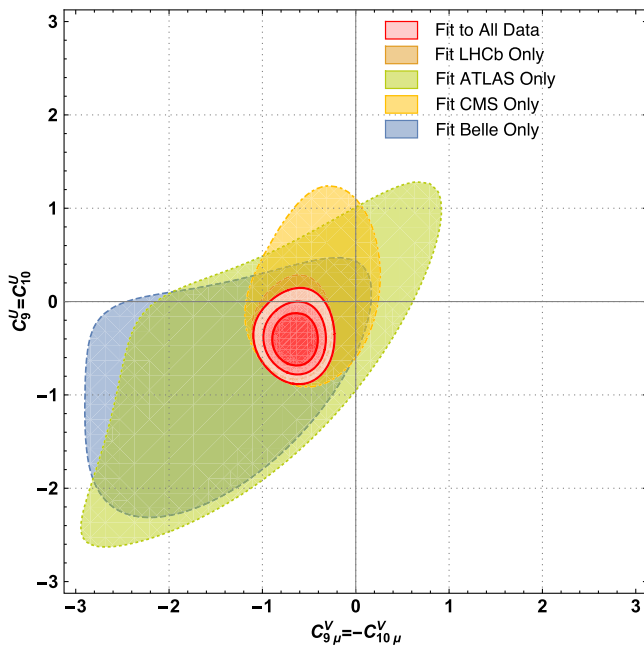
FIG. 1.　Confidence regions for scenario 6 in the plane $(\mathcal{C}^{\mathrm{V}}_{9\mu} = -\mathcal{C}^{\mathrm{V}}_{10\mu}, \mathcal{C}^{\mathrm{U}}_9 = \mathcal{C}^{\mathrm{U}}_{10})$. The regions for different experimental subsets correspond to a confidence level of 3σ, whereas the 1, 2, 3σ confidence regions are shown for the region associated with the global fit to all data.

previous results focused on LFUV NP contributions in $\mathcal{C}^{\mathrm{NP}}_{9\mu}$ without LFU NP. We consider two 2D fits:

(i) The hypothesis $\{\mathcal{C}^{\mathrm{V}}_{9\mu}, \mathcal{C}^{\mathrm{U}}_9\}$ (Table V, top) has a pull with respect to the SM of 5.7σ. The LFD observables are governed by the sum $\mathcal{C}^{\mathrm{V}}_{9\mu} + \mathcal{C}^{\mathrm{U}}_9 \simeq -1.01$ for the b.f.p., whereas the b.f.p. $\mathcal{C}^{\mathrm{V}}_{9\mu} = -1.57$ is the dominant contribution to LFUV observables. Interestingly, these results can be linked to the results of Ref. [19] (without LFU NP), with the former in agreement with the b.f.p. of the fit to all data (-1.11) in Table II of Ref. [19] and the latter closer to the b.f.p. of the fit to LFUV observables (-1.76). Therefore, the internal tension between LFD and LFUV observables in the global fit of Ref. [19] is resolved here due to the additional freedom allowed by $\mathcal{C}^{\mathrm{V}}_{9\mu}$, which enters the LFUV observables (always with a subleading contribution from $\mathcal{C}^{\mathrm{U}}_{9\mu}$), whereas the combination $\mathcal{C}^{\mathrm{V}}_{9\mu} + \mathcal{C}^{\mathrm{U}}_9$ is constrained by the LFD observables.

(ii) The hypothesis $\{\mathcal{C}^{\mathrm{V}}_{9\mu} = -\mathcal{C}^{\mathrm{V}}_{10\mu}, \mathcal{C}^{\mathrm{U}}_9\}$ (Table V, bottom) has a pull of 5.8σ and follows a similar pattern. The LFUV contribution $\mathcal{C}^{\mathrm{V}}_{9\mu} = -\mathcal{C}^{\mathrm{V}}_{10\mu} = -0.42$ (for the b.f.p.) accommodates the LFUV observables well, while the sum $\mathcal{C}^{\mathrm{V}}_{9\mu} + \mathcal{C}^{\mathrm{U}}_9 = -1.09$ takes care of the LFD observables (recovering approximately the fits to all data and to LFUV observables only from Ref. [19]).

The similar pulls with respect to the SM of the various scenarios indicate that the current measurements cannot lift the degeneracy among the hypotheses, and a different strategy should be envisaged in order to distinguish them.

IV. ROLE OF LFUV OBSERVABLES

One of the most relevant outcomes of this work is the unexpected preference for a NP solution with a prominent $\mathcal{C}^{\mathrm{NP}}_{10\ell}$ signature, both LFUV and LFU. This may represent a shift of paradigm, since until now the vast majority of global analyses performed were signaling a single NP contribution to $\mathcal{C}^{\mathrm{V}}_{9\mu}$ as the most favored solution.

The LFUV observables are natural candidates in order to identify the contributions from LFUV NP conclusively. While new and more precise measurements of R_K and R_{K^*} will certainly be useful, Refs. [19,41] pointed out the relevance of the Q_i observables (difference of optimized angular observables in muon and electron modes) and the more exotic $B_{5,6s}$ observables. Indeed, these observables are not only very clean and stringent tests against the SM, similarly to $R_{K^{(*)}}$, but they also contain additional information about the Wilson coefficients from a full angular analysis. In particular, while R_K involves crossed LFUV LFU terms such as $\mathcal{C}^{\mathrm{V}}_{9\mu}\mathcal{C}^{\mathrm{U}}_{10}$ and $\mathcal{C}^{\mathrm{V}}_{10\mu}\mathcal{C}^{\mathrm{U}}_9$, Q_5 contains a $\mathcal{C}^{\mathrm{V}}_{9\mu}\mathcal{C}^{\mathrm{U}}_9$ term, introducing complementary information to R_K; see the Appendix A.

A natural candidate to disentangle LFU and LFUV NP is then $\langle Q_5 \rangle_{[1.1,6]}$ because of its high sensitivity to $\mathcal{C}_{9\mu}^V$ and its ties to the P_5' anomaly sensitive to both types of NP contributions. $\langle R_K \rangle_{[1,6]}$ and in second place $\langle R_{K^*} \rangle_{[1,6]}$, despite the large theoretical uncertainties of the latter in the presence of NP, should also play a role due to their sensitivity to $\mathcal{C}_{10\mu}^V$. Finally, the very same $\langle P_5' \rangle_{[4,6]}$ should help discern between the LFU contributions $\mathcal{C}_9^U$ and $\mathcal{C}_{10}^U$.

We show the most interesting LFUV observables for the b.f.p. of the above scenarios in Fig. 2 (from left to right, the SM and scenarios 1 to 8). Explicit expressions of these observables are given in the Appendix A.

A decision tree can be built from the experimental measurement of $\langle Q_5 \rangle_{[1.1,6]}$, which exhibits a good discriminating power against the various scenarios considered above:

(i) If $\langle Q_5 \rangle_{[1.1,6]} \gtrsim 0.3$ (first column in Fig. 2), the 1D hypothesis $\mathcal{C}_{9\mu}^V$ is able to explain all anomalies. A confirmation can come from an updated measurement of $\langle R_{K^*} \rangle_{[1,6]} - 1 \gtrsim -0.2$ (last column in Fig. 2).

(ii) If $0.1 \lesssim \langle Q_5 \rangle_{[1.1,6]} \lesssim 0.2$, the hypotheses with only a large $\mathcal{C}_{9\mu}^{NP}$ are disfavored, while hypotheses with $\mathcal{C}_{10\mu}^V$ are favored. Actually, this range of values corresponds to solutions involving $\mathcal{C}_{9\mu}^V = -\mathcal{C}_{10\mu}^V$ (scenarios 2, 4, 6, and 8). Knowing $\langle R_K \rangle_{[1,6]}$ with an uncertainty around 5% would help discriminate between the hypotheses $\mathcal{C}_{9\mu}^V = -\mathcal{C}_{10\mu}^V$ with and without LFU contributions in $\mathcal{C}_{9\mu}^{NP}$ (scenarios 2 and 8, respectively; see the fourth
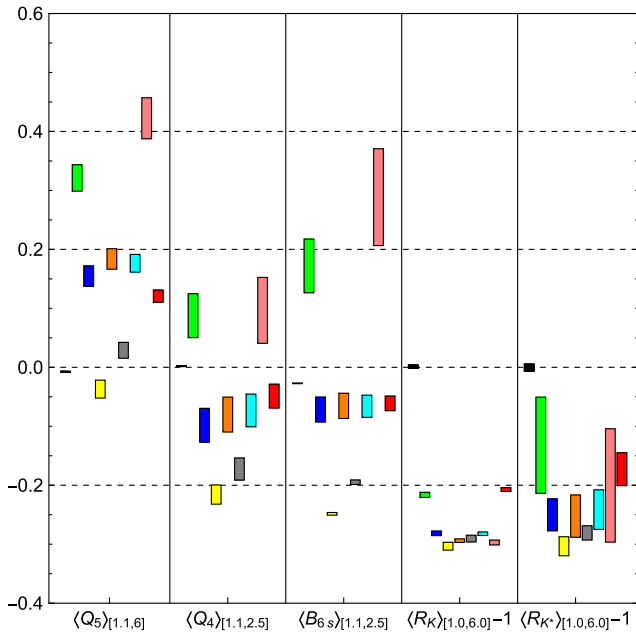
FIG. 2. Predictions for LFUV observables of interest under various hypotheses of LFU and LFUV NP contributions currently favored by the global $b \to s\ell\ell$. From left to right: the SM is followed by scenarios 1 to 8 as described in the main text. We plot $R_{K,K^*} - 1$ to keep the figure compact.

column in Fig. 2). $\langle P_5' \rangle_{[4,6]}$ can confirm this result by disentangling $\{\mathcal{C}_9^V, \mathcal{C}_{10\mu}^V\}$ from $\{\mathcal{C}_9^U = \mathcal{C}_{10\mu}^U\}$, see the Appendix C, if the experimental uncertainty on $\langle P_5' \rangle_{[4,6]}$ is reduced by half [4].

(iii) If $\langle Q_5 \rangle_{[1.1,6]} \lesssim 0.1$, scenarios in which $\mathcal{C}_{9\mu}^V$ and $\mathcal{C}_{10\mu}^V$ are left free to vary independently (scenarios 3 and 5) are preferred. Distinguishing among these two scenarios is practically impossible, since only $\langle B_{6s} \rangle_{[1.1,2.5]}$ shows a very mild discrimination power (third column in Fig. 2) if measured at a very high precision.

The value of $\mathcal{C}_{10}^U$ can be probed by $\mathcal{B}(B_s \to \ell^+\ell^-)$, assuming no significant scalar or pseudoscalar contributions:

$$\frac{\mathcal{B}(B_s \to e^+e^-)}{\mathcal{B}(B_s \to \mu^+\mu^-)} = \frac{m_e^2}{m_\mu^2} \times \frac{|\mathcal{C}_{10}^{SM} + \mathcal{C}_{10}^U|^2}{|\mathcal{C}_{10}^{SM} + \mathcal{C}_{10\mu}^V + \mathcal{C}_{10}^U|^2}. \quad (4)$$

The inclusion of $\mathcal{C}_{10}^U$ in this equation leads to and enhancement of it between 30% and 60% with respect to the SM prediction, but with strong lepton-mass suppression for this observable to be available in the near future, and similarly, assuming no large LFUV-NP contributions in $b \to s\tau\tau$, for the challenging measurement of $\mathcal{B}(B_s \to \tau^+\tau^-)$.

V. CONCLUSIONS

We have considered the current anomalies observed in $b \to s\ell\ell$ transitions and discussed the consequences of removing one hypothesis frequently made (and overlooked) in the global model-independent analyses, namely, that the anomalies are explained only by NP violating lepton–flavor universality. Instead, we explore the implications of allowing both LFU and LFUV NP contributions in the Wilson coefficients $\mathcal{C}_9$ and $\mathcal{C}_{10}$, providing more flexibility to describe the data. The LFUV observables will constrain LFUV NP contributions, whereas LFD observables will be sensitive to the sum of LFUV NP and LFU NP contributions. We found a different mechanism with a large contribution to $\mathcal{C}_{10}$ to explain the data without transgressing the $\mathcal{B}(B_s \to \mu^+\mu^-)$ constraint, leading to an improvement compared to our earlier fits restricted to LFUV NP contributions only.

The 4D hypothesis with both kinds of contributions to $\mathcal{C}_{9\ell}^{NP}$ and $\mathcal{C}_{10\ell}^{NP}$ leads to two scenarios with high significances and well-constrained parameters (equivalent to scenarios with only LFUV NP contributions and thus a more limited set of parameters). Indeed, the fits favor either a large and positive $\mathcal{C}_{10\mu}^V$ together with large and negative LFU contributions in both $\mathcal{C}_{9,10}^U$ (scenarios 3 and 5, Tables I and III) or a negative $\mathcal{C}_{9\mu}^V = -\mathcal{C}_{10\mu}^V$ together with smaller (in absolute value) but still negative LFU contributions in both $\mathcal{C}_{9,10}^U$ (scenarios 4 and 6, Tables II and IV). If LFUV lepton interactions with V − A are favored, suggesting that

$SU(2)_L$ invariance might be a guide for models for NP in $b \to s\ell\ell$, LFU lepton interactions with a V + A structure are preferred. The size and structure of these LFU lepton interactions do not agree with a generation by radiative effects from LFUV NP contributions, which leads to much smaller and purely vector LFU lepton interactions [42]. The scenarios that we discuss would also require a deviation from popular model-building ideas relying on a strong hierarchy of NP contributions according to the generations involved in order to provide a connection with $b \to c\tau\nu$ anomalies [2,36,43–50].

To separate the various scenarios explaining the $b \to s\ell\ell$ anomalies, a decision tree is proposed. Although the update of R_K will be a major milestone, the measurement of Q_5 (and the improvement of R_{K^*} and P_5') remains essential to disentangle the possible scenarios of NP and to interpret the effective description in terms of a full-fledged UV-complete model of physics beyond the Standard Model.

APPENDIX A: POLYNOMIAL PARAMETRIZATION FOR SOME OBSERVABLES OF INTEREST

The observables $\langle P_5' \rangle_{[4,6]}$, $\langle Q_5 \rangle_{[1,1,6]}$, $\langle R_K \rangle_{[1,6]}$, and $\langle R_{K^*} \rangle_{[1,6]}$ can be parametrized as follows, with the coefficients α_i for each observable collected in Table VI:

$$
\begin{aligned}
O_i = {} & \alpha_0 + \alpha_1 \mathcal{C}_9^{\mathrm{U}} + \alpha_2 \mathcal{C}_{10}^{\mathrm{U}} + \alpha_3 \mathcal{C}_{9\mu}^{\mathrm{V}} + \alpha_4 \mathcal{C}_{10\mu}^{\mathrm{V}} + \alpha_5 (\mathcal{C}_9^{\mathrm{U}})^2 \\
& + \alpha_6 (\mathcal{C}_{10}^{\mathrm{U}})^2 + \alpha_7 (\mathcal{C}_{9\mu}^{\mathrm{V}})^2 + \alpha_8 (\mathcal{C}_{10\mu}^{\mathrm{V}})^2 + \alpha_9 \mathcal{C}_9^{\mathrm{U}} \mathcal{C}_{10}^{\mathrm{U}} \\
& + \alpha_{10} \mathcal{C}_9^{\mathrm{U}} \mathcal{C}_{9\mu}^{\mathrm{V}} + \alpha_{11} \mathcal{C}_9^{\mathrm{U}} \mathcal{C}_{10\mu}^{\mathrm{V}} + \alpha_{12} \mathcal{C}_{9\mu}^{\mathrm{V}} \mathcal{C}_{10}^{\mathrm{U}} + \alpha_{13} \mathcal{C}_{9\mu}^{\mathrm{V}} \mathcal{C}_{10\mu}^{\mathrm{V}} \\
& + \alpha_{14} \mathcal{C}_{10}^{\mathrm{U}} \mathcal{C}_{10\mu}^{\mathrm{V}}.
\end{aligned}
\tag{A1}
$$

The first block in Table VI (second column) contains the Standard Model prediction. In the second block (columns 3 to 6), one can find the coefficients of the linear terms ($\mathcal{C}_9^{\mathrm{U}}$, $\mathcal{C}_{10}^{\mathrm{U}}$, $\mathcal{C}_{9\mu}^{\mathrm{V}}$, and $\mathcal{C}_{10\mu}^{\mathrm{V}}$), and the third block shows the coefficients of the quadratic terms. Since in the four observables the terms $\alpha_{6,8}$ are zero, we have not included them in Table VI.

$\langle P_5' \rangle_{[4,6]}$, being the only LFD observable in Table VI, is obviously the only observable with nonzero linear LFU terms. The combination $\mathcal{C}_9^{\mathrm{U}} + \mathcal{C}_{9\mu}^{\mathrm{V}}$ dominates $\langle P_5' \rangle_{[4,6]}$ with $\alpha_1 = \alpha_3 = -0.207$, which is approximately 25% of the SM value. The coefficients in front of $\mathcal{C}_{10,\mu}^{\mathrm{U,V}}$ verify $\alpha_{2,4} \sim 1/3\alpha_{2,3}$, while the coefficients of the quadratic terms $(\mathcal{C}_{9,\mu}^{\mathrm{U,V}})^2$ are $\alpha_{5,7} \sim \alpha_{2,4}$. Moreover, $\langle P_5' \rangle_{[4,6]}$ also has crossed terms mixing $\mathcal{C}_i^{\mathrm{U}}$ and $\mathcal{C}_{j\mu}^{\mathrm{V}}$ ($\alpha_{9\ldots14}$), even though they are subleading with respect to $\alpha_{1,3}$.

$\langle Q_5 \rangle_{[1,1,6]}$ is strongly sensitive to $\mathcal{C}_{9\mu}^{\mathrm{V}}$, with $\alpha_3 = -0.246$ being an order of magnitude larger than the rest of the coefficients. $\langle R_K \rangle_{[1,6]}$ and $\langle R_{K^*} \rangle_{[1,6]}$ are linearly sensitive to both $\mathcal{C}_{9,10\mu}^{\mathrm{V}}$, but the former only contains crossed terms mixing universal and violating contributions of the type $\mathcal{C}_{9(10)}^{\mathrm{U}} \mathcal{C}_{10(9)\mu}^{\mathrm{V}}$. Contrarily, the latter $\langle R_{K^*} \rangle_{[1,6]}$ has also quadratic terms such as $\mathcal{C}_{9(10)}^{\mathrm{U}} \mathcal{C}_{9(10)\mu}^{\mathrm{V}}$. This implies that if one sets either $\mathcal{C}_9$ or $\mathcal{C}_{10}$ to zero this kind of term remains in $\langle R_{K^*} \rangle_{[1,6]}$ while they vanish in $\langle R_K \rangle_{[1,6]}$. This difference in structure can prove useful in disentangling different scenarios.

The coefficients α_i of these parametrizations have been obtained by fitting the calculated expressions of the observables with the second-order polynomial in the Wilson coefficients in Eq. (A1). We generated the central values over a grid of values of $\mathcal{C}_{9\mu}^{\mathrm{NP}}$, $\mathcal{C}_{10\mu}^{\mathrm{NP}}$, $\mathcal{C}_{9e}^{\mathrm{NP}}$, and $\mathcal{C}_{10e}^{\mathrm{NP}}$. The grid range of the grid varied from $[-1, 1]$ for the coefficients $\mathcal{C}_{10\mu}^{\mathrm{NP}}$, $\mathcal{C}_{9e}^{\mathrm{NP}}$, and $\mathcal{C}_{10e}^{\mathrm{NP}}$ to $[-2, 2]$ for the coefficient $\mathcal{C}_{9\mu}^{\mathrm{NP}}$ (with a

TABLE VI. Coefficients of the polynomial parametrization of observables in Eq. (A1).

	α_0	α_1	α_2	α_3	α_4	α_5	α_7	α_9	α_{10}	α_{11}	α_{12}	α_{13}	α_{14}
$\langle P_5' \rangle_{[4,6]}$	−0.814	−0.207	−0.066	−0.207	−0.066	0.058	0.058	0.011	0.116	0.011	0.011	0.011	0.008
$\langle Q_5 \rangle_{[1,1,6]}$	0	0	0	−0.246	−0.019	0	0	0.033	0.066	0	0	0	0.013
$\langle R_K \rangle_{[1,6]}$	1.001	0	0	0.230	−0.264	0	0	0	0	0.061	0.061	0	0
$\langle R_{K^*} \rangle_{[1,6]}$	1.000	0	0	0.157	−0.287	0	0	0	0.042	0.045	0.045	0	−0.016

spacing of the grid of sampled points of 0.1). We stress that the above formulas correspond to central values only (the associated uncertainties could be parametrized in a similar way), but they already help identify the main sensitivities of these observables.

APPENDIX B: CORRELATIONS AMONG PARAMETERS OF THE FITS

Figure 3 shows the 1, 2, and 3σ confidence regions of the 2D fits. We also provide information about the correlations between the different parameters of each of the fits performed.

The correlations between the parameters of each fit are the following (in the order of the parameters given to describe each scenario):

(i) Scenario 3-$\{\mathcal{C}_{9\mu}^{V}, \mathcal{C}_{10\mu}^{V}, \mathcal{C}_{9}^{U}, \mathcal{C}_{10}^{U}\}$ is

$$\text{Corr}_3 = \begin{pmatrix} 1.00 & 0.59 & -0.96 & -0.52 \\ 0.59 & 1.00 & -0.56 & -0.91 \\ -0.96 & -0.56 & 1.00 & 0.48 \\ -0.52 & -0.91 & 0.48 & 1.00 \end{pmatrix}.$$

(ii) Scenario 4-$\{\mathcal{C}_{9\mu}^{V} = -\mathcal{C}_{10\mu}^{V}, \mathcal{C}_{9}^{U}, \mathcal{C}_{10}^{U}\}$ is

$$\text{Corr}_4 = \begin{pmatrix} 1.00 & -0.76 & 0.77 \\ -0.76 & 1.00 & -0.64 \\ 0.77 & -0.64 & 1.00 \end{pmatrix}.$$

(iii) Scenario 5-$\{\mathcal{C}_{9\mu}^{V}, \mathcal{C}_{10\mu}^{V}, \mathcal{C}_{9}^{U} = \mathcal{C}_{10}^{U}\}$ is

$$\text{Corr}_5 = \begin{pmatrix} 1.00 & 0.88 & -0.93 \\ 0.88 & 1.00 & -0.92 \\ -0.93 & -0.92 & 1.00 \end{pmatrix}.$$

(iv) Scenario 6-$\{\mathcal{C}_{9\mu}^{V} = -\mathcal{C}_{10\mu}^{V}, \mathcal{C}_{9}^{U} = \mathcal{C}_{10}^{U}\}$ is

$$\text{Corr}_6 = \begin{pmatrix} 1.00 & -0.01 \\ -0.01 & 1.00 \end{pmatrix}.$$

(v) Scenario 7-$\{\mathcal{C}_{9\mu}^{V}, \mathcal{C}_{9}^{U}\}$ is

$$\text{Corr}_7 = \begin{pmatrix} 1.00 & -0.93 \\ -0.93 & 1.00 \end{pmatrix}.$$

(vi) Scenario 8-$\{\mathcal{C}_{9\mu}^{V} = -\mathcal{C}_{10\mu}^{V}, \mathcal{C}_{9}^{U}\}$ is

$$\text{Corr}_8 = \begin{pmatrix} 1.00 & -0.47 \\ -0.47 & 1.00 \end{pmatrix}.$$

The 4D fit (scenario 3) exhibits very strong anticorrelations between $\mathcal{C}_{9\mu}^{V}$ and $\mathcal{C}_{9}^{U}$ and between $\mathcal{C}_{10\mu}^{V}$ and $\mathcal{C}_{10}^{U}$. This is logical since $b \to s\mu^+\mu^-$ constrains $\mathcal{C}_{i\mu}^{V} + \mathcal{C}_{i}^{U}$ while $b \to se^+e^-$ constrains $\mathcal{C}_{i}^{U}$ and the LFUV observables constrain $\mathcal{C}_{i\mu}^{V}$. In fact, without LFUV observables, we would find a correlation of -1 between $\mathcal{C}_{i\mu}^{V}$ and $\mathcal{C}_{i}^{U}$ because the LFD observables only see the sum of both types of contributions. The same pattern can be observed in the
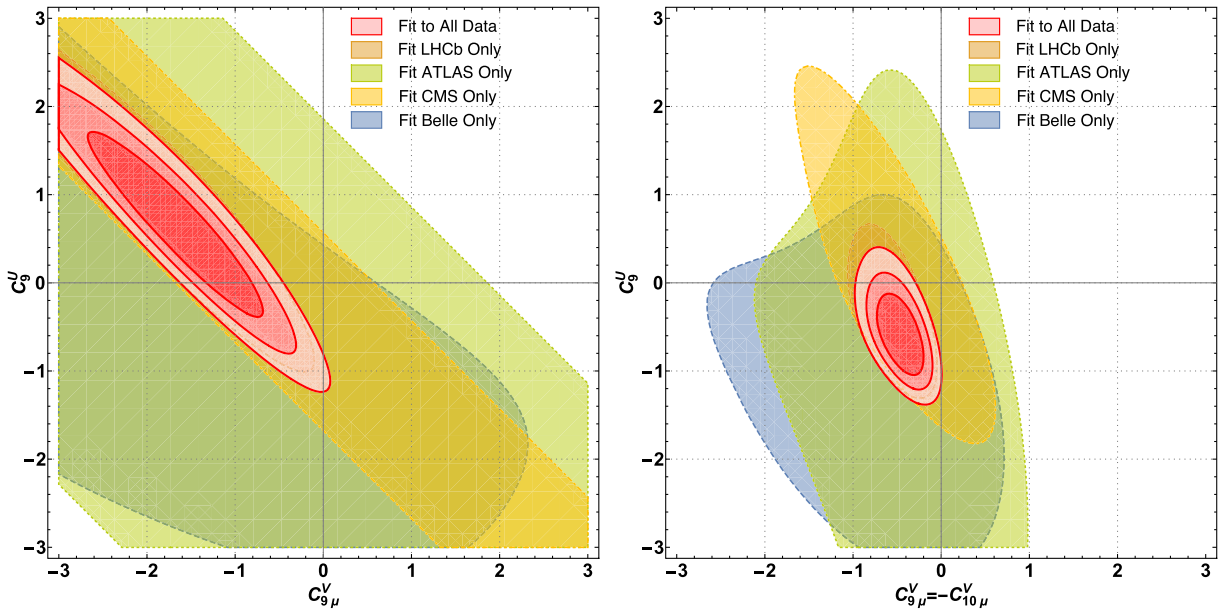
FIG. 3.   Left: Correlation between $\mathcal{C}_{9\mu}^{V}$ and $\mathcal{C}_{9}^{U}$ from the scenario 7 fit. Right: Correlation between the parameters $\mathcal{C}_{9\mu}^{V} = -\mathcal{C}_{10\mu}^{V}$ and $\mathcal{C}_{9}^{U}$ from the scenario 8 fit. The regions for different experimental subsets correspond to a confidence level of 3σ, whereas the 1, 2, 3σ confidence regions are shown for lepton region associated with the global fit to all data.

other fits, although correlations are nominally less strong due to the fact that different and more involved structures, like $\mathcal{C}_{9\mu}^{V} = -\mathcal{C}_{10\mu}^{V}$, are explored.

One should also stress that the correlation between the parameters $\mathcal{C}_{9\mu}^{V} = -\mathcal{C}_{10\mu}^{V}$ and $\mathcal{C}_{9}^{U} = \mathcal{C}_{10}^{U}$ in scenario 6 is negligible, signaling its statistical independence. This means that the underlying structure of most of the LFD observables is such that, when imposing $\mathcal{C}_{9\mu}^{V} = -\mathcal{C}_{10\mu}^{V}$, once its value is fitted to the LFUV observables, the parameter $\mathcal{C}_{9}^{U} = \mathcal{C}_{10}^{U}$ can be independently determined by the LFD observables.

APPENDIX C: FURTHER TESTS

Figure 4 is a visual account of the decision tree discussed in the main text: in the case of an experimental determination of $\langle Q_5 \rangle_{[1.1,6]}$ finding a value close to 0.4 with enough precision (green band), only a solution involving $\mathcal{C}_{9\mu}^{NP}$ (blue lines) can explain both $\langle Q_5 \rangle_{[1.1,6]}$ and $\langle R_K \rangle_{[1,6]}$. However, this test has no discriminating power if $\langle Q_5 \rangle_{[1.1,6]}$ is measured to be around 0.2 (blue band), since both $\mathcal{C}_{9\mu}$ and $\mathcal{C}_{9\mu} = -\mathcal{C}_{10\mu}$ (red lines) scenarios could then explain $\langle Q_5 \rangle_{[1.1,6]}$ and $\langle R_K \rangle_{[1,6]}$. Another remarkable feature of this test is its robustness against its sensitivity to LFU NP contributions. The solid curves in Fig. 4 correspond to $\langle R_K \rangle_{[1,6]}(\langle Q_5 \rangle_{[1.1,6]})$, assuming there are no LFU contributions to the Wilson coefficients, while the dotted curves are realizations of the same functions but including
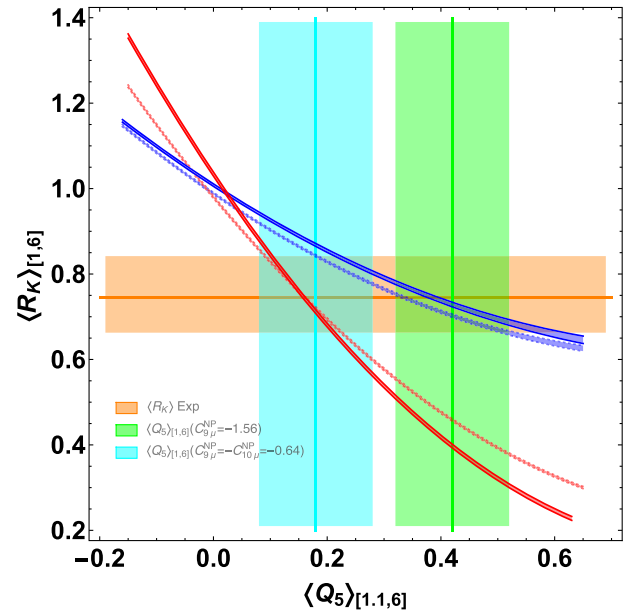
FIG. 4. $\langle R_K \rangle_{[1,6]}$ as a function of $\langle Q_5 \rangle_{[1.1,6]}$ in the four of the scenarios analyzed. The solid blue and solid red lines correspond to $\mathcal{C}_{9,10}^{U} = 0$, while the dotted blue and dotted red lines have LFU contributions $\mathcal{C}_{9}^{U} = 0.56$ and $\mathcal{C}_{9}^{U} = \mathcal{C}_{10}^{U} = -0.44$, respectively.

contributions of the size suggested by our fits. As expected from the structure of the observables used in these tests, the inclusion of LFU NP contributions barely induces corrections in the shapes of the curves.

[1] T. Blake, T. Gershon, and G. Hiller, Annu. Rev. Nucl. Part. Sci. **65**, 113 (2015).

[2] S. Bifani, S. Descotes-Genon, A. Romero Vidal, and M. H. Schune, J. Phys. G **46**, 023001 (2019).

[3] Y. Amhis *et al.* (HFLAV Collaboration), Eur. Phys. J. C **77**, 895 (2017).

[4] S. Descotes-Genon, L. Hofer, J. Matias, and J. Virto, J. High Energy Phys. 06 (2016) 092.

[5] R. Aaij *et al.* (LHCb Collaboration), Phys. Rev. Lett. **111**, 191801 (2013).

[6] R. Aaij *et al.* (LHCb Collaboration), J. High Energy Phys. 02 (2016) 104.

[7] R. Aaij *et al.* (LHCb Collaboration), Phys. Rev. Lett. **113**, 151601 (2014).

[8] R. Aaij *et al.* (LHCb Collaboration), J. High Energy Phys. 07 (2013) 084.

[9] R. Aaij *et al.* (LHCb Collaboration), J. High Energy Phys. 08 (2017) 055.

[10] (ATLAS Collaboration), CERN Report No. ATLAS-CONF-2017-023, 2017.

[11] (CMS Collaboration), CERN Report No. CMS-PAS-BPH-15-008, 2017.

[12] A. Abdesselam *et al.* (Belle Collaboration), arXiv:1604.04042.

[13] S. Wehle *et al.* (Belle Collaboration), Phys. Rev. Lett. **118**, 111801 (2017).

[14] A. Khodjamirian, T. Mannel, A. A. Pivovarov, and Y.-M. Wang, J. High Energy Phys. 09 (2010) 089.

[15] S. Descotes-Genon, L. Hofer, J. Matias, and J. Virto, J. High Energy Phys. 12 (2014) 125.

[16] B. Capdevila, S. Descotes-Genon, L. Hofer, and J. Matias, J. High Energy Phys. 04 (2017) 016.

[17] C. Bobeth, M. Chrzaszcz, D. van Dyk, and J. Virto, Eur. Phys. J. C **78**, 451 (2018).

[18] S. Descotes-Genon, J. Matias, and J. Virto, Phys. Rev. D **88**, 074002 (2013).

[19] B. Capdevila, A. Crivellin, S. Descotes-Genon, J. Matias, and J. Virto, J. High Energy Phys. 01 (2018) 093.

[20] W. Altmannshofer, P. Stangl, and D. M. Straub, Phys. Rev. D **96**, 055008 (2017).

[21] L. S. Geng, B. Grinstein, S. Jager, J. M. Camalich, X. L. Ren, and R. X. Shi, Phys. Rev. D **96**, 093006 (2017).

[22] M. Ciuchini, A. M. Coutinho, M. Fedele, E. Franco, A. Paul, L. Silvestrini, and M. Valli, Eur. Phys. J. C **77**, 688 (2017).

[23] G. D'Amico, M. Nardecchia, P. Panci, F. Sannino, A. Strumia, R. Torre, and A. Urbano, J. High Energy Phys. 09 (2017) 010.

[24] A. Arbey, T. Hurth, F. Mahmoudi, and S. Neshatpour, Phys. Rev. D **98**, 095027 (2018).

[25] G. Buchalla, A. J. Buras, and M. E. Lautenbacher, Rev. Mod. Phys. **68**, 1125 (1996).

[26] A. J. Buras, arXiv:hep-ph/9806471.

[27] J. Matias, F. Mescia, M. Ramon, and J. Virto, J. High Energy Phys. 04 (2012) 104.

[28] S. Descotes-Genon, T. Hurth, J. Matias, and J. Virto, J. High Energy Phys. 05 (2013) 137.

[29] W. Altmannshofer, P. Ball, A. Bharucha, A. J. Buras, D. M. Straub, and M. Wick, J. High Energy Phys. 01 (2009) 019.

[30] M. Beneke, T. Feldmann, and D. Seidel, Nucl. Phys. **B612**, 25 (2001).

[31] T. Huber, E. Lunghi, M. Misiak, and D. Wyler, Nucl. Phys. **B740**, 105 (2006).

[32] A. J. Buras and M. Munz, Phys. Rev. D **52**, 186 (1995).

[33] C. Greub, V. Pilipp, and C. Schupbach, J. High Energy Phys. 12 (2008) 040.

[34] T. Blake, U. Egede, P. Owen, K. A. Petridis, and G. Pomery, Eur. Phys. J. C **78**, 453 (2018).

[35] R. Aaij *et al.* (LHCb Collaboration), J. High Energy Phys. 04 (2015) 064.

[36] D. Buttazzo, A. Greljo, G. Isidori, and D. Marzocca, J. High Energy Phys. 11 (2017) 044.

[37] W. Buchmuller and D. Wyler, Nucl. Phys. **B268**, 621 (1986).

[38] B. Grzadkowski, M. Iskrzynski, M. Misiak, and J. Rosiek, J. High Energy Phys. 10 (2010) 085.

[39] R. Alonso, B. Grinstein, and J. Martin Camalich, Phys. Rev. Lett. **113**, 241802 (2014).

[40] A. Celis, J. Fuentes-Martin, A. Vicente, and J. Virto, Phys. Rev. D **96**, 035026 (2017).

[41] B. Capdevila, S. Descotes-Genon, J. Matias, and J. Virto, J. High Energy Phys. 10 (2016) 075.

[42] A. Crivellin, C. Greub, F. Saturnino, and D. Müller, Phys. Rev. Lett. **122**, 011805 (2019).

[43] B. Capdevila, A. Crivellin, S. Descotes-Genon, L. Hofer, and J. Matias, Phys. Rev. Lett. **120**, 181802 (2018).

[44] S. L. Glashow, D. Guadagnoli, and K. Lane, Phys. Rev. Lett. **114**, 091801 (2015).

[45] B. Bhattacharya, A. Datta, D. London, and S. Shivashankara, Phys. Lett. B **742**, 370 (2015).

[46] R. Alonso, B. Grinstein, and J. Martin Camalich, J. High Energy Phys. 10 (2015) 184.

[47] L. Calibbi, A. Crivellin, and T. Ota, Phys. Rev. Lett. **115**, 181801 (2015).

[48] S. Fajfer and N. Kosnik, Phys. Lett. B **755**, 270 (2016).

[49] M. Bauer and M. Neubert, Phys. Rev. Lett. **116**, 141802 (2016).

[50] D. Becirevic, S. Fajfer, N. Kosnik, and O. Sumensari, Phys. Rev. D **94**, 115021 (2016).